Macromolecular Bioscience
www.mbs-journal.de

3D Microfibrous Scaffolds Selectively Promotes Proliferation and Glial Differentiation of Adult Neural Stem Cells: A Platform to Tune Cellular Behavior in Neural Tissue Engineering

*Bhavika B. Patel, Farrokh Sharifi, Daniel P. Stroud, Reza Montazami, Nicole N. Hashemi, and Donald S. Sakaguchi**

Biomaterials are essential for the development of innovative biomedical and therapeutic applications. Biomaterials-based scaffolds can influence directed cell differentiation to improve cell-based strategies. Using a novel microfluidics approach, poly (ε-caprolactone) (PCL), is used to fabricate microfibers with varying diameters (3–40 μm) and topographies (straight and wavy). Multipotent adult rat hippocampal stem/progenitor cells (AHPCs) are cultured on 3D aligned PCL microfibrous scaffolds to investigate their ability to differentiate into neurons, astrocytes, and oligodendrocytes. The results indicate that the PCL microfibers significantly enhance proliferation of the AHPCs compared to control, 2D planar substrates. While the AHPCs maintained their multipotent differentiation capacity when cultured on the PCL scaffolds, there is a significant and dramatic increase in immunolabeling for astrocyte and oligodendrocyte differentiation when compared with growth on planar surfaces. Our results show a 3.5-fold increase in proliferation and 23.4-fold increase in astrocyte differentiation for cells on microfibers. Transplantation of neural stem/progenitor cells within a PCL microfiber scaffold may provide important biological and topographic cues that facilitate the survival, selective differentiation, and integration of transplanted cells to improve therapeutic strategies.

1. Introduction

Severe brain injury as well as neurodegenerative conditions, often lead to life-long disability, reduced quality of life, and heavy social as well as economic burdens. As such, considerable effort has been directed toward the development of cell replacement strategies in animal models to investigate nervous system repair.[1–4] Further, genetically engineered cells can secrete neurotrophic factors thus providing a neuroprotective benefit to a site of injury.[5–8] However, when cells are transplanted, the outcome often results in poor cell survival, poor host integration, and little functional benefit due to the complexity of the central nervous system (CNS). Therefore, there is an urgent need to develop innovative techniques to increase the efficiency for transplantation therapies.

Biomaterials have emerged as an innovative and powerful adjunct in support of brain rescue and repair strategies. Studies have shown an improvement in cell engraftment using biomaterial supports, which resulted in increased cell survival.[9,10] Various scaffolds can be placed into a site of injury in order to provide structural and architectural support to damaged brain tissue. Biomaterials, such as microfibers, can mimic the cellular microenvironment and can support cell adhesion, proliferation, and differentiation. Scaffolds can serve as cellular delivery platforms incorporating extracellular matrix (ECM) molecules, natural polymers, or synthetic polymers, offering new ways to develop more effective transplantation therapies for the nervous system.[11–13]

Recently, microfluidic platforms have shown promise to a wide range of applications from biomedical to energy areas.[14–20] Microfluidic fiber fabrication is versatile, straightforward, cost-effective, and biocompatible. Furthermore, this approach does not require high temperature, pressure, and voltage to fabricate fibers as is necessary for conventional methods.[21–24] Additionally, the microfluidic platform can be applied to create other bioactive materials, such as particles, liposomes, droplets, and vesicles.[25,26]

B. B. Patel, Dr. D. S. Sakaguchi
Department of Genetics
Development, and Cell Biology and Neuroscience Program
Iowa State University
Ames, IA 50011, USA
E-mail: dssakagu@iastate.edu
Dr. F. Sharifi, Dr. R. Montazami, Dr. N. N. Hashemi
Department of Mechanical Engineering
Iowa State University
Ames, IA 50011, USA
D. P. Stroud, Dr. D. S. Sakaguchi
Department of Genetics
Development, and Cell Biology, Biology Program
Iowa State University
Ames, IA 50011, USA
The ORCID identification number(s) for the author(s) of this article can be found under https://doi.org/10.1002/mabi.201800236.

DOI: 10.1002/mabi.201800236

Using poly (ε-caprolactone) (PCL) fibrous scaffolds has two main advantages. PCL can be considered as a good candidate for long-term implantable devices due to its slow degradation rate compared to other synthetic polymers, like poly(lactic-co-glycolic acid) (PLGA), making the microenvironment less acidic during the degradation process.[27] Additionally, PCL fibers can be fabricated without a cross-linking process. Therefore, the resulting fibers have high strain at break and are not likely to fragment easily during implantation.

The discovery and characterization of adult neural stem/progenitor cells has been influential in understanding brain regenerative capabilities. Adult neural stem/progenitor cells (NPCs) are located in two main regions in the brain, the dentate gyrus of the hippocampus and the subventricular zone.[28] The ability of these cells to differentiate into neurons, astrocytes, and oligodendrocytes, the principal neural cell types of the CNS, provides an advantage for studying directed cell differentiation.[29] Combined with biomaterials, scaffolds can also influence cell differentiation thus promoting stem cells into neural lineages for therapeutic strategies for nervous system rescue and repair.[30–35] However, little is known about the extent to which PCL microfibers may impact cell proliferation and directed cell differentiation.

Our group previously showed PCL microfibers can support adult hippocampal stem/progenitor cell (AHPC) proliferation and differentiation.[16] In the present study, we extend our previous observations and have conducted a systematic and quantitative characterization of the effect of microfluidic-spun PCL microfibers of varying sizes and topographies on AHPC proliferation and differentiation. In order to investigate these issues, we found the microfluidic approach provides excellent versatility for fabricating PCL fibers with a wide range of characteristics. We demonstrated that by changing the flow rate ratio between the core and sheath fluids, as well as PCL concentration (in the core fluid), we were able to achieve wavy and straight fibers with different sizes. These architectures have been previously fabricated using various techniques and in different size ranges; however, for our specific application of creating a 3D microenvironment to enhance neural progenitor cell differentiation into glial cells, using fibers in similar size range of cells is preferred.[36–38] After culturing the AHPCs on the microfibrous scaffolds of various diameters and topographies, we found that the larger diameter microfibers appear to guide the differentiation to mature neurons, whereas all PCL microfibers promoted astrocyte differentiation. We demonstrated that PCL microfibers promote cell proliferation and influence differentiation to varying degrees. By investigating new platforms for cell transplantation, we are in a better position to understand how to improve the survival, differentiation, and integration of transplanted cells for nervous system rescue and repair.

2. Results

2.1. Microfiber Fabrication and Properties

A schematic of our microfluidic fiber fabrication platform is illustrated in **Figure 1**. In this process, PCL solidification is due to the solvent extraction process. Following convergence of the sheath and core fluids in the channel, the molecules of the sheath fluid are exchanged with the molecules of the core fluid and PCL precipitates due to the insolubility of PCL in the sheath fluid. In this process, the sheath fluid plays a pivotal role in exerting lateral and vertical hydrodynamics focusing forces on the core fluid. The chevron region focuses the core fluid vertically. In this area, the hydrodynamic resistance in the perpendicular direction (to the flow) decreases and the sheath fluid fills the top and bottom of the microchannel, exerting vertical and lateral forces, to wrap around the core fluid, and focuses the core fluid at the center of the microchannel. The sheath fluid fills the chevron areas because the hydrodynamic resistance is inversely related to the flow rate and we used significantly higher flow rates for the sheath fluid, blocking the core fluid from entering the chevron areas. This creates a shear force at the core fluid/sheath fluid interface due to the velocity and viscosity difference between the two fluids, which plays an important role to place the core fluid at the center of the channel, change the cross-section as well as the topographies of the resulting fiber, and align the polymer chain in the flow direction. In addition to the fiber fabrication process, Figure 1 schematically shows the impact of shear force at the fluid/fluid interface on the pattern of the PCL fibers.

Scanning electron micrographs illustrate the ability of the microfluidic approach to create fibers with different topographies such as straight (**Figure 2**A–C) and wavy (Figure 2D,E) with different diameters. By changing the flow rate ratio (FRR) between the core and sheath fluids, as well as PCL concentration (in the core fluid), we were able to achieve architectures that have not been reported in other fiber fabrication studies including the microfluidic approach. Details about the PCL concentration and FRR used are provided in **Table 1**.

The microfluidic fiber fabrication process is dependent on finding the range of flow rate ratios between the core and sheath fluids which allow for the continuous formation of fibers. For this study, different flow rates ratios (sheath flow rate:core flow rate) were tested in order to find the best flow rate range (50:10 to 200:2). If the flow rate ratio was lower than five (50:10), the lateral focusing force from the sheath fluid was not enough to keep the core fluid at the center of the microchannel. Thus, the core fluid attached the walls of the microchannel and would quickly block it. Conversely, when higher flow rates were used, the phase inversion process was too rapid and resulted in sudden solidification of PCL when it was exposed to the sheath fluid in the microchannel and blockage occurred again. Additionally, if the FRR was higher than 100 (200:2), the back-flow effect was observed in the channel, as the lateral shear force exerted from the sheath fluid to the core fluid was sufficient enough that the sheath fluid blocked the core fluid from entering the main part of the microchannel where the two fluids should meet. Instead, the sheath fluid would flow back to the core fluid channel, which caused early solidification of PCL and channel blockage.

Although the FRR plays a significant role on the size, cross-sectional and lateral shapes (straight and wavy) of the fibers, this parameter has a limited effect on fiber shape and structure. This limitation prevented the fabrication of straight fibers in

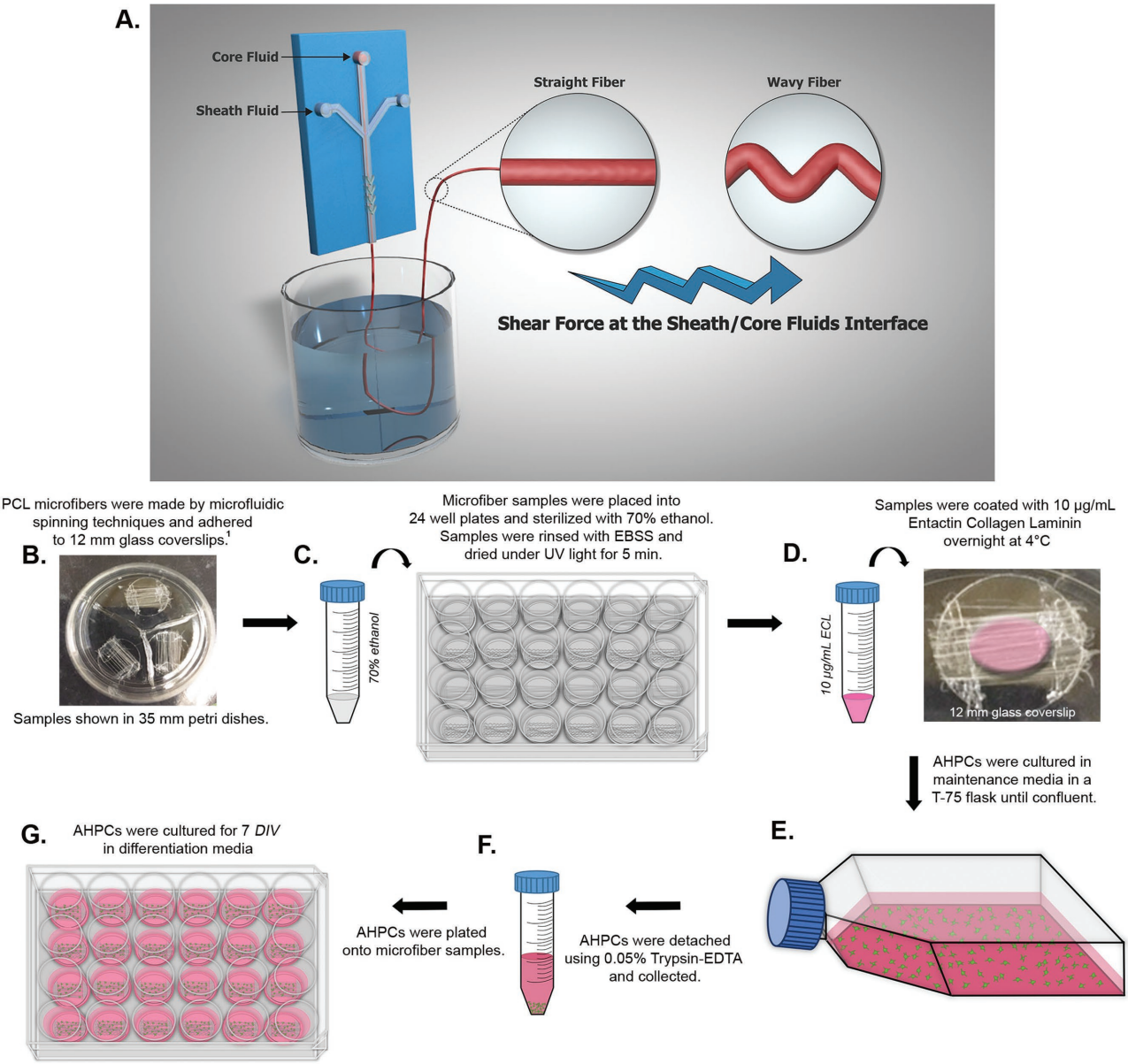

Figure 1. A) Schematic of microfluidic fiber fabrication process and the effect of shear force, at the sheath/core fluids at the fluid/fluid interface, on the topography of the resulting fibers. B) Microfibers placed in a 35 mm petri dish. C) Sterilized using 70% ethanol. D) ECL diluted in DMEM/F-12 at a concentration of 10 µg mL^{-1}. E) AHPCs cultured in T-75 flask until 80% confluent, F) cells collected using trypsin, and G) cultured on ECL-coated microfiber and control samples for 7 DIV in differentiation media.

the size range of 20–30 µm in this study. In fact, by decreasing the FRR to five (50:10), the size of the fiber increased to 39 µm and the fiber shape changed from wavy to straight. In order to create straight fibers within the size range of 20–30 µm (Straight II), the PCL concentration, another important parameter, was reduced to 2% from 5% and the size of the resulting Straight II was found to decrease to 22.8 µm from 39 µm (Straight III). Decreasing the concentration of PCL reduces the mass solidification rate in the core fluid during the phase inversion process within the microchannel.

This table shows that the Straight I microfibers can be created by using a high FRR between the core and sheath fluids that result in high shear force at the interface. When the FRR decreases to the range of 18–30, the wavy shaped fibers were created and the diameter of the fibers increased. The decrease of the FRR to 50:10, gives Straight III PCL fibers with the diameter of 39.1 ± 1.8 µm.

2.2. Cell Adhesion on PCL Microfibers

To assess cellular adhesion, AHPCs were cultured on PCL microfibers precoated with an extracellular matrix substrate (entactin-collagen-laminin IV [ECL]) for 7 days in vitro (DIV)

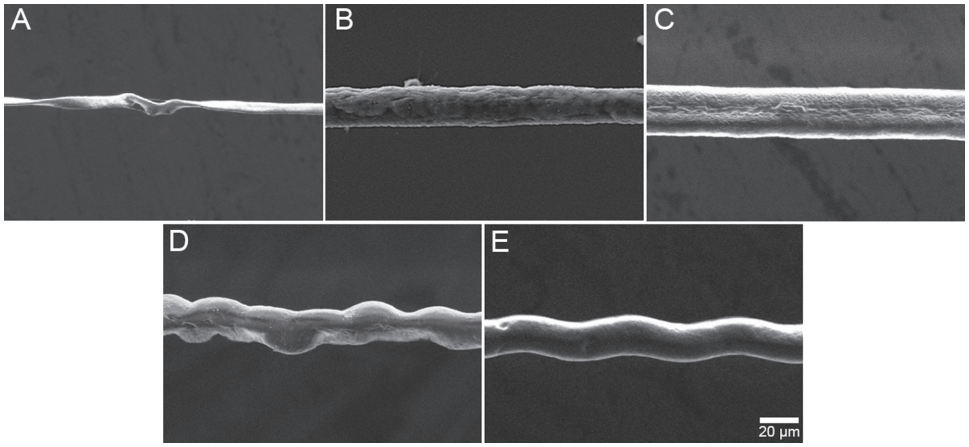

Figure 2. Scanning electron microscope images of the microfluidic-spun PCL fibers fabricated with different patterns of A) Straight I. B) Straight II. C) Straight III. D) Wavy I. E) Wavy II. Scale bar = 20 µm.

in differentiation media (DM). Neural stem cells in vitro are cultured on an extracellular matrix substrate such as laminin. Previous studies have shown that using an extracellular matrix substrate aids in cell adhesion, specifically on fiber matrices.[32,39,40] The details of our in vitro study are illustrated in Figure 1B–E. For comparison, cells were also grown on a planar surface of ECL-coated glass coverslips. The AHPCs were stained with DAPI, a nuclear stain, in order to perform cell counts and to assess differences of cell density on PCL microfibers versus planar controls. Our results show that PCL microfibers permit AHPC adhesion and Straight I microfibers had the highest cell density, with a mean of 10 325 cells per mm^2 (**Figure 3**A_1–E_1,F).

Straight I microfibers bundled together, therefore increasing the surface area and allowing more cells to attach and cluster together (**Figure 4**A_1–A_3, Figure S1A_1–A_2, Supporting Information). Further, Straight II microfibers had more clusters of cells (Figure 4B_1–B_3) compared to Straight III microfibers (Figure 4C_1–C_3), which is likely due to the lower overall cell density on the Straight III microfibers. Interestingly, cells growing on Wavy I microfibers were evenly distributed and cell processes often followed the curvatures of the fibers (Figure 4D_1–D_3,E_1–E_3). These results indicate that not only do PCL microfibers support cell adhesion, but also fiber diameters influence cell density.

2.3. Proliferation of AHPCs on Microfiber Substrates

In order to determine if cell proliferation was impacted by the PCL microfibers, we conducted Ki-67 immunolabeling. The Ki-67 antigen is expressed in the cell nucleus during G1, S, G2, and M phases of the cell cycle. As illustrated in **Figure 5**, significantly greater percentages of AHPCs were Ki-67 immunolabeled on microfiber samples compared to the planar controls. Ki-67 immunolabeling was 2.7- to 3.5-fold greater on the microfibers compared to the planar controls (Figure 5A_1–E_1,F). The percentage of Ki-67-immunolabeled AHPCs on microfiber samples were found to be 10.8% ± 1.3, 10.5% ± 1, 9.5% ± 1, 12.1% ± 1.4, and 11.3% ± 1, (Straight I, Straight II, Straight II, Wavy I, and Wavy II), respectively, compared to planar controls which only showed 3.5% ± 0.3 Ki-67 positive immunolabeled cells (Figure 5A_1–E_1,F). These results indicate that PCL microfibers provide structural support that helps promote cell proliferation.

Propidium iodide (PI) staining was used to determine if there was any significant cell death of the AHPCs when growing on the PCL microfibers. Propidium iodide (PI) is a fluorescent nuclear and chromosome counterstain that is membrane impermeant and is commonly used to identify dead cells. In our study, we found few PI-positive cells on the microfibers (Figure S2, Supporting Information). As a PI reagent

Table 1. Details of the PCL concentration and flow rate ratio (FRR) used to fabricate PCL microfibers with different patterns and diameters.

PCL concentration [w/v%]	Sheath:core flow rate ratio (FRR)	Pattern	Diameter (± SEM) [µm]	Median [µm]	Minimum [µm]	Maximum [µm]
5	200:2	Straight I	3 ± 0.11	2.8	1.2	6.8
2	150:10	Straight II	22.8 ± 0.84	23.5	8.5	42.1
5	50:10	Straight III	39.1 ± 0.60	39	25.3	58.4
5	150:5	Wavy I	26.5 ± 0.49	26	16.9	39.9
5	90:5	Wavy II	29.3 ± 0.76	27.5	16	49

Abbreviation: SEM, standard error of the mean. $N = 3$ independent experiments for a total of 90 imaging fields analysed.

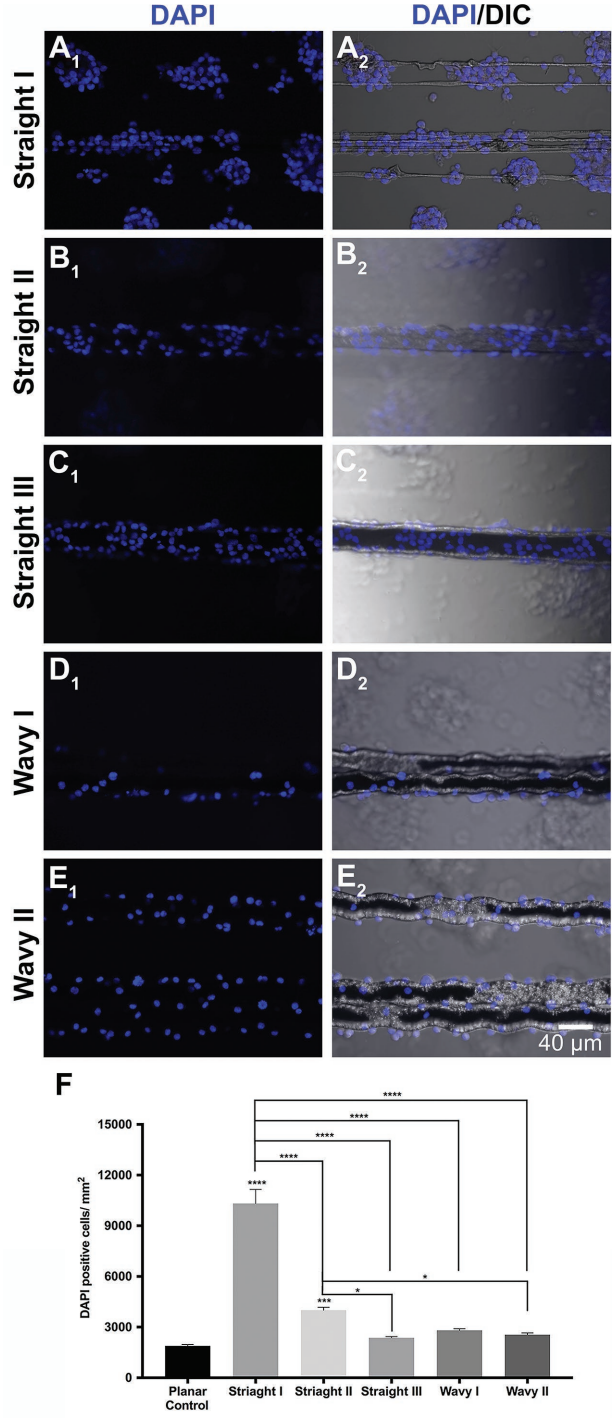

Figure 3. Images depicting cell density of AHPCs growing on PCL microfibers. Straight I microfiber samples had a higher cell density versus all other microfiber types including the planar control samples. A_1–E_1) AHPCs stained with DAPI on various PCL microfiber diameters. A_2–E_2) DAPI merged with DIC images. Scale bar = 40 µm. Abbreviations: DAPI, 4′,6-diamidino-2-phenylindole; DIC, differential interference contrast. F) Quantitative analysis of cell density on various microfiber samples. Error bars represent standard error of the mean. $N = 18$ independent experiments for a total of 90 imaging fields. *Significantly different at $p \leq 0.05$. ***Significantly different at $p \leq 0.01$. ****Significantly different at $p \leq 0.0001$.

positive control, AHPCs were incubated in 70% ethanol for 5 min (Figure S2A_1–A_3, Supporting Information), a condition effective at killing most of the cells. These results show that all microfiber substrates supported cell survival and caused negligible cell death (Figure S2B–F, Supporting Information).

2.4. AHPCs Maintain Neural Progenitor Status on PCL Microfibers

AHPCs are neural stem cells, expressing a specific class of intermediate filament proteins. An antibody directed against nestin, a class of intermediate filament proteins found in NPCs, was used to identify the AHPCs. Previous studies have inferred that as neural precursors begin to differentiate, they are likely to express markers indicative of precursor cells, such as nestin. Hence, although cells are differentiating, they maintain expression of nestin during early stages of the differentiation process.[41,42] Fluorescent images showed the majority of cells were immunopositive for nestin in the cell body and processes (Figure S3A_1–E_1, Supporting Information). No statistically significant differences were noted between microfiber samples and planar controls (Figure S3F, Supporting Information). These results indicate that the growth of AHPCs on microfiber samples did not alter their progenitor status. Along with data previously shown, these results indicate that PCL microfibers provide structural support that does not alter AHPC progenitor state but enhances cell proliferation, ideal for cell transplantation strategies. Adult hippocampal progenitor cells with processes oriented in the direction of the microfiber as well as the contour of the microfiber were commonly observed on different types of fibers as shown in Figure S4A_1–E_2, Supporting Information. Figure S4F, Supporting Information shows the average (average ± standard error) of the neurite length corresponding to the AHPCs growing in one direction. Wavy fibers had longer neurite lengths than straight fibers; however, no statistical differences was found.

2.5. PCL Microfibers Support Neuronal Differentiation

The AHPCs are multipotent and have the capacity to differentiate into neurons, astrocytes, and oligodendrocytes.[29] Scaffolds can influence cell differentiation, which can be used to help promote targeted stem cell differentiation toward specific neural lineages as a therapeutic strategy for nervous system rescue and repair.[11,12] Using immunocytochemistry, neuronal differentiation was characterized using neuron-specific antibody markers, TuJ1 (class III β-tubulin) and MAP2ab (microtubule associated protein 2ab). AHPCs on microfibers and planar surfaces were immunopositive for TuJ1 but no significant differences were observed on any microfibers ($p \leq 0.05$), suggesting that although PCL microfibers may not increase neuronal differentiation, they support the ability of AHPCs to differentiate (**Figure 6**A_1–E_1,K). Mature neurons can be identified using the anti-MAP2ab antibody, specific to microtubules within dendrites.[16] The number of cells immunoreactive for MAP2ab on Straight III microfibers was significantly greater than planar controls, 14% ± 1.8 versus 6.3% ± 0.6, respectively

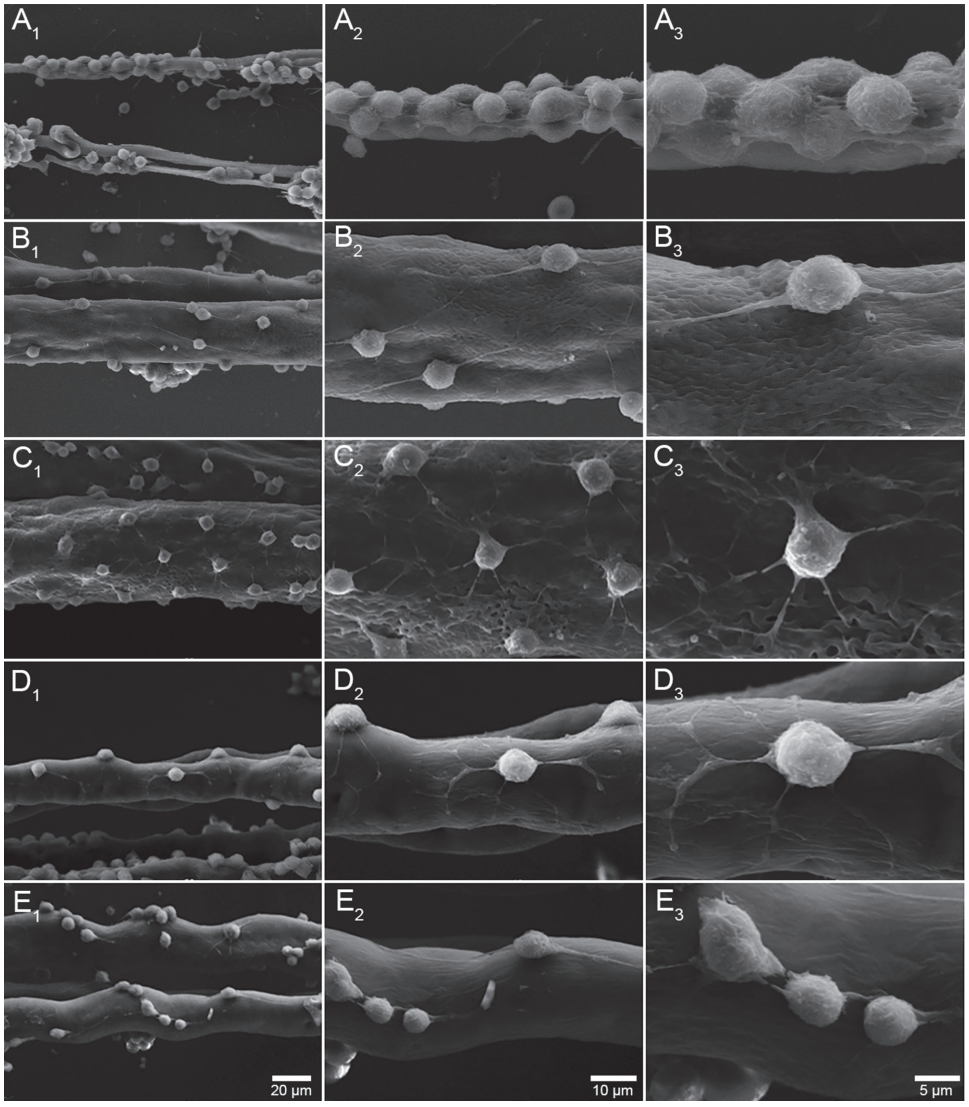

Figure 4. SEM images of the AHPCs aligned on the surface of different diameters and shapes of the microfluidic-spun PCL fibers after 7 days in vitro. A_1–A_3) Straight I: 5% PCL and FRR is 200:2. B_1–B_3) Straight II: 2% PCL and FRR is 150:10. C_1–C_3) Straight III: 5% PCL and FRR is 50:10. D_1–D_3) Wavy I: 5% PCL and FRR is 150:5. E_1–E_3) Wavy II: 5% PCL and FRR is 90:5. A_1–E_1) Scale bar = 20 μm. A_2–E_2) Scale bar = 10 μm. A_3–E_3) Scale bar = 5 μm.

(Figure $6F_1$–J_1,K), suggesting that specific topographies, surface and scaffold diameters, may help promote neuronal differentiation and maturation.

2.6. PCL Microfibers Enhance Glial Differentiation of AHPCs

To determine if PCL microfibrous scaffolds stimulate glial differentiation, glial fibrillary acidic protein (GFAP) and receptor interacting protein (RIP) were used to characterize astrocytes and oligodendrocytes, respectively. Our results indicate a dramatic increase in the number of cells immunopositive for GFAP on all microfiber samples compared to the controls, ranging from a 16.7- to 23.4-fold increase. Fluorescent images show distinct immunolabeling in long processes and these cells appeared to have larger nuclei compared to cells that were negative for GFAP. On Straight I microfibers, distinct processes can be seen following the fiber length (**Figure 7**A_1,F_1). When growing on Wavy I and II microfibers, the glial processes often followed the contours of crests and troughs compared to those GFAP positive cells on Straight microfibers that appear to have linear processes. Quantitative analysis revealed the percentage of GFAP immunoreactivity of AHPCs on microfiber samples were 17.9% ± 2.163, 18.2% ± 2, 15.9% ± 2.2, 17.4% ± 3.6, and 13.1% ± 2.5, respectively (Figure $7A_1$–E_1,K). AHPCs differentiating on all PCL microfibers showed a remarkable increase in GFAP immunolabeling compared to the very low percentage (0.8%) on planar surfaces further indicating that PCL microfibers promote glial differentiation. Differentiation of AHPCs into oligodendrocytes was greater on the larger microfiber samples showing the highest RIP immunoreactivity of all PCL microfibers. RIP immunoreactivity was found in many

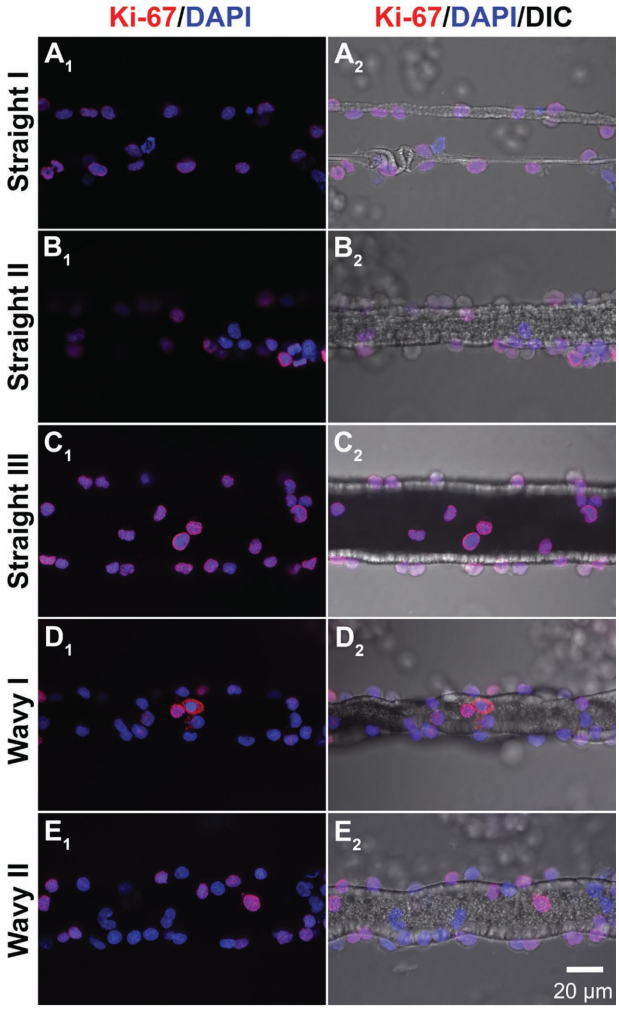

Figure 5. Proliferation of AHPCs on PCL microfibers. A_1–E_1) Fluorescent images of AHPCs illustrating immunoreactivity for Ki-67 on various PCL microfiber diameters: Ki-67-Cy3 (red) with DAPI staining (blue). A_2–E_2) Ki-67-Cy3 and DAPI merged with DIC. Scale bar = 20 µm. Abbreviations: DAPI, 4′,6-diamidino-2-phenylindole; DIC, differential interference contrast. F) Quantitative analysis of proliferation of AHPCs immunoreactive for Ki-67 antibody. Error bars represent standard error of the mean. $N = 3$ experiments, five imaging fields per experiment. **Significantly different at $p \leq 0.001$. ****Significantly different at $p \leq 0.0001$.

short processes emanating from the cell bodies. Straight III and Wavy II, (Figure $7H_1$,J_1) showed significant differences in the number of RIP immunoreactive cells compared to planar controls, 27% ± 3.6 and 21.7% ± 2.5 (Figure $7F_1$–J_1,K). Further, Wavy II microfibers (larger diameter) are shown to have more RIP immunolabeled cells than Straight I microfibers (small diameter), suggesting that AHPCs can be biased toward oligodendrocyte differentiation on larger microfibers with a wavy topography. Taken together, these results indicate that microfluidic spun PCL microfibers increase glial differentiation, favoring astrocytic differentiation of the AHPCs.

2.7. AHPCs Bridge across PCL Microfibers

The regenerative capacity of the CNS is limited, requiring sequential complex processes in which axons must make their way through a prohibitive glial scar and subsequently navigate to find their correct target region, or result in neuronal death.[17] An important step in the regenerative process involves the axons crossing the lesion site. Biomaterials can serve as bridges in which cells are able to migrate and extend processes, in hopes of reaching their target. Although AHPCs often formed mini-clusters reminiscent of neurospheres on Straight I microfibers (Figure $S4A_1$–A_2, Supporting Information), larger diameter microfibers displayed AHPCs bridging between fibers as illustrated in Figures S4 and S5, Supporting Information. In many cases, the microfibers were separated by more than 80 µms (Figure $S4B_1$–E_2, Supporting Information). These results were further validated in immunocytochemical experiments where cell bodies were often localized on one microfiber with its processes extending across and intricately wrapping around a nearby PCL microfiber (Figure $S5A_1$–C_1, Supporting Information). These results show that microfibers can support cells bridging between fibers, therefore forming an aligned scaffolding system useful for cell migration, alignment, and structural organization during development and regeneration.

3. Discussion

We have successfully shown that biocompatible PCL microfibers support the adhesion and differentiation of AHPCs. Most importantly, the PCL microfibers promoted proliferation of the AHPCs compared to a 2D surface and have shown that PCL microfibers considerably enhance glial differentiation. An increased number of AHPCs were immunoreactive for GFAP, an astrocyte-specific class-III intermediate filament protein. Astrocytes are a major cell type in the mammalian nervous system. In addition to providing metabolic and nutritional support to their partner neurons, they also play important functions during development, including neuronal guidance, supporting proliferation and maintenance of neurons, stimulating neurogenesis, involvement in synaptogenesis and neurotrophic support due to their paracrine activities.[18] To our knowledge, for the first time, the 3D microenvironment of PCL microfibers greatly enhanced neural progenitor cell differentiation into glial cells.

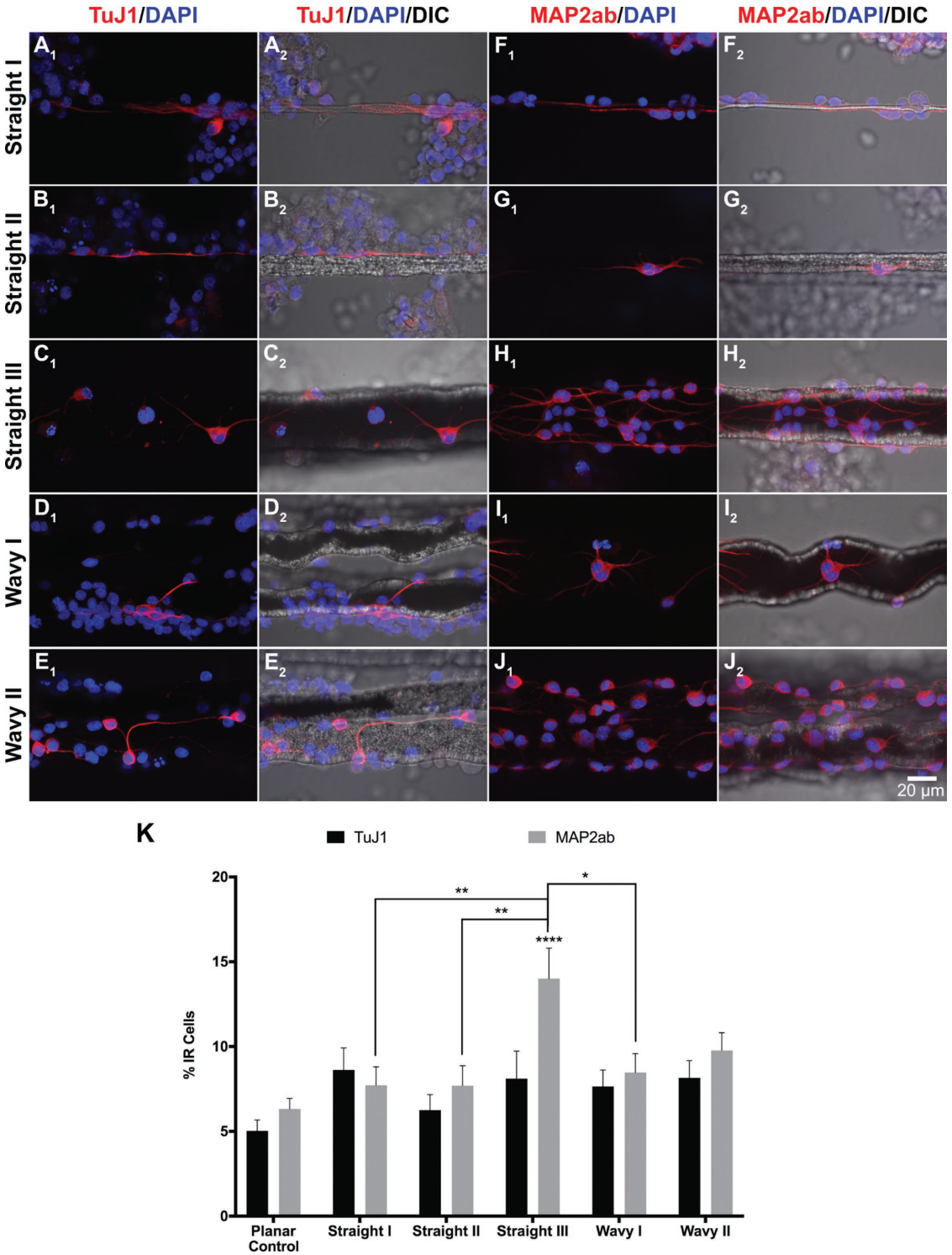

Figure 6. Neuronal differentiation on PCL microfibers. A_1–E_1) Fluorescent images of AHPCs immunolabeled for TuJ1 on various PCL microfiber samples: TuJ1-Cy3 (red) with DAPI staining (blue). A_2–E_2) TuJ1-Cy3 and DAPI merged with DIC. F_1–J_1) Fluorescent images of AHPCs immunolabeled for MAP2ab on various PCL microfiber samples: MAP2ab-Cy3 (red) with DAPI staining (blue). F_2–J_2) MAP2ab-Cy3 and DAPI merged with DIC. Scale bar = 20 µm. Abbreviations: TuJ1, βIII-tubulin; MAP2ab, microtubule associated protein 2ab; DAPI, 4′,6-diamidino-2-phenylindole; DIC, differential interference contrast. K) Quantitative analysis of neuronal differentiation of AHPCs immunoreactive for TuJ1 or MAP2ab antibodies. Error bars represent standard error of the mean. $N = 3$ independent experiments, five imaging fields quantified per experiment. *Significantly different at $p \leq 0.01$. **Significantly different at $p \leq 0.002$. ****Significantly different at $p \leq 0.0001$.

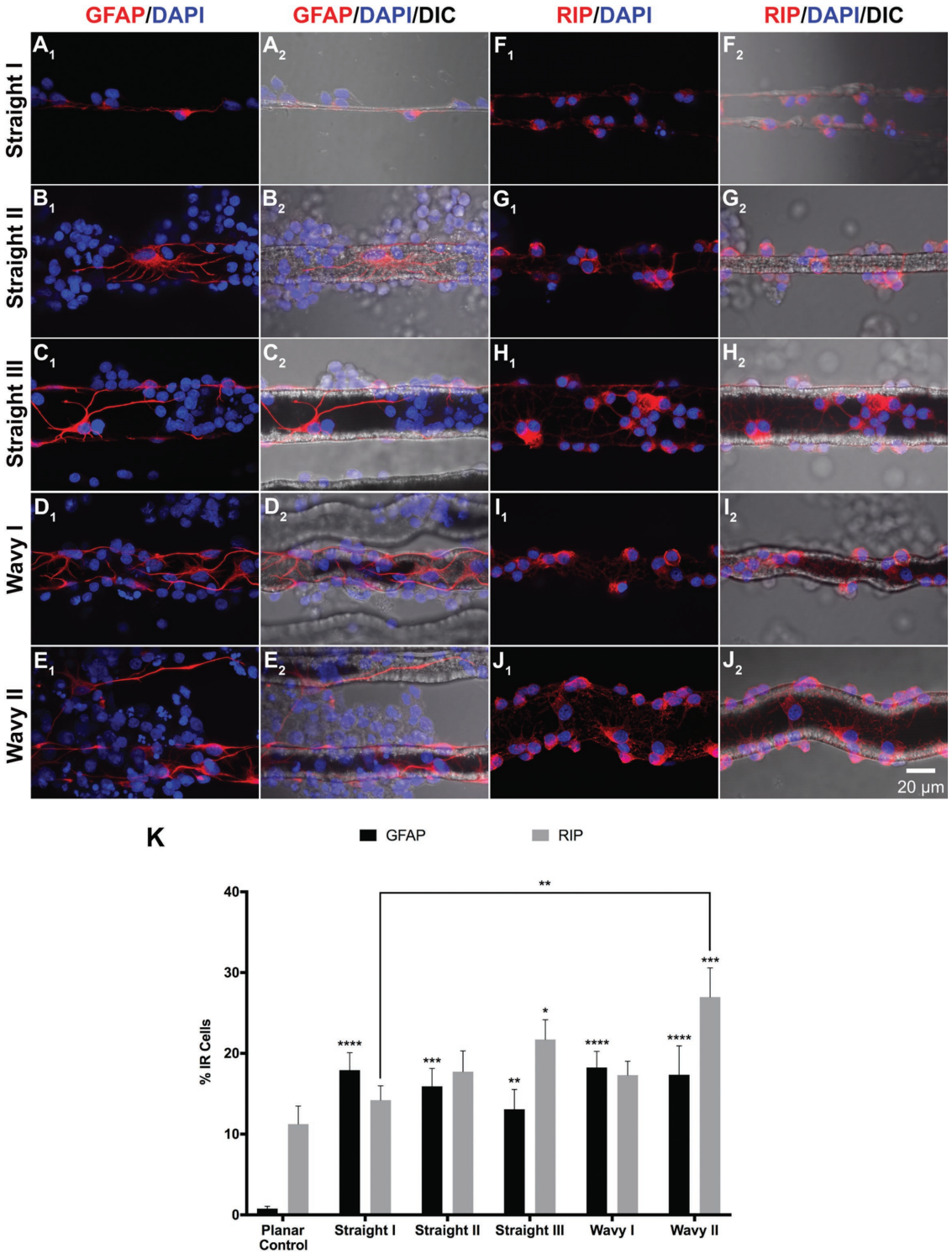

Figure 7. Glial differentiation on PCL microfibers. A_1–E_1) Fluorescent images of AHPCs illustrating immunoreactivity for GFAP on various PCL microfiber samples: GFAP-Cy3 (red) with DAPI staining (blue). A_2–E_2) GFAP-Cy3 and DAPI merged with DIC. F_1–J_1) Fluorescent images of AHPCs illustrating immunoreactivity for RIP on various PCL microfiber samples: RIP-Cy3 (red) with DAPI staining (blue). F_2–J_2) RIP-Cy3 and DAPI merged with DIC. Scale bar = 20 µm. Abbreviations: GFAP, glial fibrillary acidic protein; RIP, receptor interacting protein; DAPI, 4′,6-diamidino-2-phenylindole; DIC, differential interference contrast. K) Quantitative analysis of glial differentiation of AHPCs immunoreactive for GFAP or RIP antibodies. Error bars represent standard error of the mean. $N = 3$ independent experiments, five imaging fields per experiment. *Significantly different at $p \leq 0.05$. **Significantly different at $p \leq 0.0058$. ***Significantly different at $p \leq 0.0002$. ****Significantly different at $p \leq 0.0001$.

3.1. Microfibrous Scaffolds

Microfibrous scaffolds have shown promise for serving as ideal drug carriers due to their high surface area to volume ratio and tunable morphologies.[17] We used both of the parameters involved in the microfluidic fiber fabrication, that is, PCL concentration and FRR, and were able to fabricate different types of fibers with a wide range of sizes. In the process of microfluidic fiber fabrication, core and sheath fluids were introduced into the microchannel, as described in the experimental section. Using the laminar flow regime, the diffusion occurred at the sheath/core fluids interface. In this paper, we showed that we could tune the shear force by changing the velocity and viscosity gradients at the interface, which resulted in different microfiber patterns: straight and wavy. These fiber topographies were expected since decreasing the shear force at the interface, resulted in fabrication of microfibers displaying a transition pattern between the straight and wavy microfibers. Depending on the flow rate ratio and the PCL concentration, chain shaped microfibers could also be fabricated. Additionally, because the flow rate ratio decreases, the hydrodynamic focusing force weakens and the core fluid expands in the channel, which results in the fabrication of fibers with larger diameters. To obtain straight PCL fibers with smaller diameters, it was necessary to adjust the flow rate ratio but also change the PCL concentration in the core fluid, another important parameter affecting the size of the PCL fibers. Therefore, we used a lower concentration of PCL in the core fluid, that is, 2 w/v%, which resulted in PCL fibers with smaller diameters after the phase inversion process and the exchange of molecules of the sheath fluid with the molecules of the core fluid in the microchannel. In this study, the diameter of the microfibers ranged from 3 to 40 μm, and we investigated the effect of fiber diameter as well as topography of the fibers on cellular behavior such as cell proliferation and neuronal/glial differentiation.

AHPCs are capable of differentiating into neuronal and glial cells in vitro.[41,43] In vivo, the local microenvironment plays important roles in maintaining the neural stem cell niche in order to regulate the their proliferation and differentiation.[44–46] Previously, our lab has shown that AHPCs on micropatterned polymer substrates favor neuronal differentiation compared to planar surfaces, even in the presence of soluble factors from astrocytes, indicating that surface topography played a fundamental role in neuronal differentiation.[33,47] Our current study focused on further characterizing the AHPCs on PCL microfibers to better understand the differentiation and proliferation of the cells in an in vitro model.

3.2. Scaffolds for Cell Differentiation

Due to inefficiencies in cell transplantation alone, studies have begun to implement different biomaterials to support transplanted cells and to increase their survivability. Neural progenitor cell transplants have been used in various neurodegenerative disease models including Parkinson's disease, spinal cord injury, and Huntington's disease. However, these cells have low integration efficiency into the brain circuitry, which may prevent long-term positive outcomes. In recent years, studies have started focusing on using scaffolds in order to direct cells toward specific lineages.[48–50] Additional studies have shown improvement of cell adhesion as well as differentiation of retinal progenitor cells seeded on polymeric scaffolds in a retinal degeneration model.[50–52] Taken together, studies have utilized biocompatible materials in order to investigate mechanisms to promote cellular proliferation and differentiation.

One obstacle researchers face throughout in vitro studies is mimicking the native tissue present in the brain due to the lack of cell to extracellular matrix (ECM) interactions. However, biomaterials can serve as a way to mimic the ECM that is present in vivo. These PCL microfibers promoted the differentiation of the AHPCs toward glial lineages (GFAP–astrocytes and RIP–oligodendrocytes). In addition to their crucial roles in regulating neuronal function, astrocytes also respond to CNS injury.[53] Astrocytes become activated during injury and form a glial scar to provide protection but can also increase inflammation in some neurological diseases, including Alzheimer's.[54,55]

PCL microfibers may provide topographic and guidance cues, which promote cell proliferation and glial differentiation. Along with biochemical signals, cells also regulate their behavior using mechanical stimuli from their local microenvironment.[56,57] Mechanical properties of the ECM are of growing interest because in vivo, cells are within a 3D matrix of varying properties such as stiffness and geometry, both of which can be manipulated using biomaterials. In this way, biomaterials provide an experimental model in vitro to study cell directionality, migration, and motility.

4. Conclusions

A microfluidic platform was used to fabricate PCL fibrous scaffold with a wide range of size and patterns in order to study their effects on cellular behavior. Our results have shown promise in being able to promote cell proliferation and glial cell differentiation. Combining cellular therapeutic strategies with biomaterials can provide a necessary and more conducive environment with structural support for cells to survive, proliferate, and differentiate into specific cell lineages that can be used for CNS rescue and repair.

5. Experimental Section

Microfluidic Channel Fabrication: The channel was created using a SU8 photoresist-patterned silicon wafer and soft lithography. In order to make the channel with its chevron grooves extending from the top and bottom of the channel, we used two silicon wafers. The height and width of the microchannel was 130 and 390 μm, respectively. The microchannel included four chevrons with dimensions of 130 μm × 100 μm (height × width), which were spaced 200 μm apart. The microchannel was made of polydimethylsiloxane (PDMS; Dow Corning, Midland, MI), a biocompatible and transparent elastomer. To make the channel, Sylgard 184 elastomer base and cross-linker agents were mixed in a 10:1 ratio. After pouring the mixture on the molds, it was cured at 85 °C for 25 min. Then, the PDMS layers were simply peeled off from the silicon wafer molds and bonded together via plasma treatment.

Microfluidic Fiber Fabrication: To fabricate microfibers we used two fluids,that is, core and sheath fluids. The core fluid was prepared with poly(ε-caprolactone) (Mn = 80 000) (PCL; Sigma-Aldrich, St. Louis, MO)

with concentrations of 2 and 5 w/v% in 2,2,2-trifluoroethanol (TFE; Oakwood Chemical, West Columbia, SC). For example, in order to make 5 w/v% PCL, 2 g of PCL were dissolved in 40 mL TFE at room temperature. The sheath fluid solution was made by using 5 w/v% polyethylene glycol (Mn = 20 000) (PEG; Sigma-Aldrich) in the mixture of ethanol and deionized (DI) water with a volume ratio of 1:1. Both of the core and sheath fluids were introduced into the three inlet microchannel using a double syringe pump (ColeParmer, Veron Hills, IL) with different flow rates, and the PCL fiber was fabricated due to the phase inversion process. In this process, the molecules of the sheath and core fluids are replaced and because PCL is not soluble in the sheath fluid, it precipitates in a form of microfibers (solvent extraction process). The position of the microchannel is vertical such that the outlet of the channel is in contact with a water bath. The production rate can vary based on the flow rates of the core and sheath fluids and the resulting fiber was collected around a frame in an aligned manner.

Microfiber Substrate Preparation: Microfiber substrate samples were prepared as previously described.[16] Briefly, each PCL fiber apparatus was composed of a 12 mm glass coverslip (Thermo Fisher Scientific, Waltham, MA), aligned PCL microfibers fixed at their ends to the coverslip via silicone medical adhesive, and small shards of fragmented coverslip to hold the ends of the microfibers in place in conjunction with the adhesive. Twelve millimeter coverslips were cleaned with RBS 35 detergent (1:50 in deionized water H_2O; Thermo Fisher Scientific) and boiled for 15 min followed by a rinse in DI water. Coverslips were air dried and sterilized under ultraviolet light. A small drop of silicone medical adhesive was applied to opposing ends of a sterile coverslip and then an array of horizontal and parallel PCL microfibers was placed onto the coverslip so that both ends lay in the adhesive. Fragments of coverslip were pressed onto the adhesive to securely bind the fibers to the coverslip. This leaves the ends of the microfiber array bound to the coverslip while the center of the array is loose from the coverslip in order to provide a 3D cell culture condition on the fibrous scaffolds. After the adhesive dried, the samples were sterilized in 70% ethanol for 20 min and washed in Earle's balanced salt solution (EBSS; Invitrogen, Carlsbad, CA). EBSS was then aspirated off and the samples were further sterilized in ultraviolet light for 10 min. Samples were incubated overnight at 4 °C with ECL (10 µg mL^{-1}; Millipore, Billerica, MA) diluted in Dulbecco's modified Eagle's medium/Ham's F-12 (DMEM/F12, 1:1, Omega Scientific, Tarzana, CA). The next day, samples were rinsed with EBSS and ready for cell plating.

Cell Culture: The adult rat hippocampal stem/progenitor cells (AHPCs) were a generous gift from F.H Gage (Salk Institute for Biological Sciences in La Jolla, CA). The AHPCs were isolated from Fischer 344 rats and were infected with a retrovirus to induce expression of green fluorescent protein (GFP).[41] During the course of the experiments, it was evident that AHPCs were decreasing the expression of the GFP transgene, which may be attributed to cell differentiation. However, this did not affect the proliferation or survival of the cells.

Cells were cultured in flasks coated with poly-L-ornithine (10 µg mL^{-1}; Sigma-Aldrich) and purified mouse laminin (5 µg mL^{-1}; R&D Systems, Minneapolis, MN) diluted in EBSS. Maintenance media (MM) was composed of DMEM/F12, 1:1 supplemented with 2.5 mM L-alanyl-L-glutamine (GlutaMAX; Thermo Fisher Scientific), N2 supplement (Gibco BRL, Gaithersburg, MD), and 20 ng mL^{-1} basic fibroblast growth factor (human recombinant bFGF; Promega Corporation, Madison, WI). Cells were detached from the culture flask using 0.05% trypsin-EDTA (Gibco BRL), the cell suspension collected and centrifuged at 800 rpm for 5 min. A hemocytometer and Trypan Blue were used to perform a viable count cells. AHPCs were plated at a density of 50 000 cells on each PCL microfiber sample. Cells were maintained at 37 °C in 5% CO_2/95% humidified air atmosphere. After 1 day in culture, differentiation was induced by growth factor withdrawal (differentiation medium, DM) and cells cultured for an additional 6 days. For feeding, half of the media was changed every other day.

For control samples, 12 mm glass coverslips were coated with ECL (10 µg mL^{-1}) overnight at 4 °C. AHPCs were plated at a density of 10 000 cells on each control sample. After 1 day in culture, differentiation was induced by growth factor withdrawal (differentiation medium, DM) and cells cultured for an additional 6 days. For feeding, half of the media was changed every other day.

Immunocytochemistry: Cultured cells were rinsed in 0.1 M phosphate buffer and fixed with 4% paraformaldehyde (PFA, Thermo Fisher Scientific) in 0.1 M phosphate buffer for 20 min at room temperature. The PFA was then aspirated off and cells were washed with phosphate buffered saline (PBS; Invitrogen). Next, cells were incubated for 1 h at room temperature in a blocking solution composed of PBS supplemented with 2.5% normal goat serum and 2.5% normal donkey serum (Jackson ImmunoResearch, West Grove, PA), 0.4% bovine serum albumin (BSA; Sigma-Aldrich), and 0.2% Triton X-100 (Thermo Fisher Scientific). Cells were then incubated overnight at 4 °C in primary antibodies diluted in blocking solution (Table S1, Supporting Information). The next day, cells were washed with PBS and followed by incubation at room temperature for 90 min in secondary antibodies (donkey anti-rabbit Cy3 or donkey anti-mouse Cy3 [1:500; Jackson ImmunoResearch] and 4',6-diamidino-2-phenylindole [DAPI] nuclear stain [1:50; Invitrogen] all diluted in blocking solution). Samples were mounted on microscope slides with DAPI Fluoromount-G mounting media (Southern Biotech, Birmingham, AL) for imaging.

Sample Preparation for SEM Imaging: After 7 days in vitro (DIV), samples were fixed and rinsed in 0.1 M phosphate buffer. Samples were then placed in a solution of water and PBS at a ratio of 50:50 for 10 min and dehydrated in a graded ethanol series (increasing ethanol concentration by 10% increments). Once samples were in 100% ethanol, samples were rinsed in a 3:1 solution of ethanol and hexamethyldisilazane (HMDS; Electron Microscopy Sciences, Hatfield, PA). The ratio of HMDS gradually increased from 25% to 100%. The ratio of ethanol:HMDS changed from 3:1 to 1:1 and 1:3, each for 10 min. The final step was to add 100% HMDS and allow the samples to air-dry overnight.

Propidium Iodide Assay: Propidium iodide (PI, Thermo Fisher Scientific) staining was used to detect dead cells at 7 DIV. The stock solution of PI was diluted to 1.5 µM in AHPC culture medium. Culture medium from each sample was replaced with the PI solution and samples were incubated for 20 min at 37 °C in 5% CO_2/95% humidified air atmosphere. As a reagent control, several samples were incubated in 70% ethanol for 5 min to cause cell death prior to the addition of the PI solution. Following incubation, samples were rinsed with 0.1 M phosphate buffer and then fixed with 4% PFA in 0.1 M phosphate buffer for 30 min at room temperature. Next, samples were rinsed with PBS and incubated for 30 min at room temperature with DAPI (1:50) diluted in blocking solution. Samples were then rinsed with PBS and mounted on microscope slides with DAPI Fluoromount-G mounting media for imaging.

Imaging: Immunocytochemistry samples were imaged using a Nikon Microphot FXA (Nikon Corp., Melville, NY, USA) microscope equipped with standard epifluorescence illumination and a Q imaging Retiga 2000R (Q Imaging, Burnaby, BC, Canada) digital camera. A 20× objective was used to obtain images for quantitative data analysis. For the analysis, ten microscopic fields were imaged per microfiber sample, each field representing 0.24 mm^2. A total of three independent culturing experiments were conducted, with a total of 15 images quantified per antibody, per microfiber sample.

A Zeiss LSM700 Confocal microscope equipped with an AxioCam MRc5 was used to image samples for high-resolution images with 20× and 40× objectives. Stacks of various optical planes were taken for each microfiber type. Using ImageJ, z-stacks were rendered into maximum intensity projections to obtain a single image. In order to create movies using the z-series of images, ImageJ was used to open the image sequence and save as an audio video interleave file.

Scanning electron microscopy (SEM; JCM-6000 NeoScope Benchtop scanning electron microscope) was used to determine the size and surface properties of the PCL fibers as well as the distribution and position of the AHPCs on fibers. The substrates were iridium (Ir)-coated (5 nm thickness) using a Q150T Turbo-Pumped Sputter Coater/Carbon Coater.

Quantitative Data Analysis: ImageJ software was used to analyze the images. From each replicate, five imaging fields were chosen per sample for each primary antibody. To calculate cell density, DAPI-stained nuclei were counted on microfibers. The length and diameter of the microfiber were measured in pixels with a ratio of 1.66 pixels to 1 µm. These values were then converted to the surface area of one half of a cylinder (imaged surface of the microfiber) using the equation surface area = $\pi\times$ (diameter in mm) $\times$ (length in mm) $\times$ 0.5. The number of DAPI stained cells was divided by the microfiber surface area to determine cell density.

After immunocytochemical experiments and imaging, quantitative analysis was conducted. Five imaging fields were examined from microfiber samples and five imaging samples were examined for planar controls. The following counts were made in each field to determine the percentage of immunolabeled cells for each respective antibody: total number of immunolabeled cells divided by the total number of cells (DAPI-stained nuclei) (see Table S1, Supporting Information).

Statistics: GraphPad Prism v6 software (GraphPad Software, Inc., La Jolla, CA, USA) was used for statistical analysis. One-way ANOVA was used to compare the means across the various conditions for cell density, anti-nestin, and Ki-67 antibodies. Two-way ANOVA was used to compare the means across the various conditions for anti-TuJ1, MAP2ab, GFAP, and RIP antibodies. A p-value of ≤ 0.05 was considered significant. Error bars represent the standard error of the mean.

Supporting Information

Supporting Information is available from the Wiley Online Library or from the author.

Acknowledgements

This work was partially supported by the Stem Cell Research Fund, the Department of Genetics, Development, and Cell Biology, the Office of Naval Research (ONR), Grant N000141612246, ONR Grant N000141712620, Iowa State College of Engineering Exploratory Research Project and US Army Medical Research and Materiel Command. The authors would like to thank Dr. F. Gage at the Salk Institute for the gift of the AHPCs. Grace Herzberg, a current student in the Biological and Pre/Medical Illustration Program (BPMI) at Iowa State University, did the graphical abstract. A special thanks to Emily Kozik, a SULI intern from the Ames Laboratory for her work during the summer and Marissa Roghair for her schematic illustration in Figure 1.

Conflict of Interest

The authors declare no conflict of interest.

Keywords

3D microfibrous scaffolds, biomaterials, glial differentiation, neural stem cells, polycaprolactone, regenerative medicine

Received: June 21, 2018
Revised: September 28, 2018
Published online: November 27, 2018

[1] S. J. Van Hoffelen, M. J. Young, M. A. Shatos, D. S. Sakaguchi, *Invest. Opthalmol. Vis. Sci.* **2003**, *44*, 426.
[2] Y. Guo, P. Saloupis, S. J. Shaw, D. W. Rickman, *Invest. Opthalmol. Vis. Sci.* **2003**, *44*, 3194.
[3] B. J. Cummings, N. Uchida, S. J. Tamaki, D. L. Salazar, M. Hooshmand, R. Summers, F. H. Gage, A. J. Anderson, *Proc. Natl. Acad. Sci.* USA **2005**, *102*, 14069.
[4] A. Iwanami, S. Kaneko, M. Nakamura, Y. Kanemura, H. Mori, S. Kobayashi, M. Yamasaki, S. Momoshima, H. Ishii, K. Ando, Y. Tanioka, N. Tamaoki, T. Nomura, Y. Toyama, H. Okano, *J. Neurosci. Res.* **2005**, *80*, 182.
[5] M. M. Harper, S. D. Grozdanic, B. Blits, M. H. Kuehn, D. Zamzow, J. E. Buss, R. H. Kardon, D. S. Sakaguchi, *Invest. Opthalmol. Vis. Sci.* **2011**, *52*, 4506.
[6] M. Sasaki, C. Radtke, A. M. Tan, P. Zhao, H. Hamada, K. Houkin, O. Honmou, J. D. Kocsis, *J. Neurosci.* **2009**, *29*, 14932.
[7] C. P. Hofstetter, E. J. Schwarz, D. Hess, J. Widenfalk, A. El Manira, D. J. Prockop, L. Olson, *Proc. Natl. Acad. Sci.* USA **2002**, *99*, 2199.
[8] A. D. Sharma, P. A. Brodskiy, E. M. Petersen, M. Dagdeviren, E. A. Ye, S. K. Mallapragada, D. Sakaguchi, *J. Vis. Exp.* **2015**, *95*, e52242.
[9] B. G. Ballios, M. J. Cooke, L. Donaldson, B. L. Coles, C. M. Morshead, D. van der Kooy, M. S. Shoichet, *Stem Cell Rep.* **2015**, *4*, 1031.
[10] T. Y. Wang, J. S. Forsythe, D. R. Nisbet, C. L. Parish, *Biomaterials* **2012**, *33*, 9188.
[11] S. K. Mallapragada, T. M. Brenza, J. M. McMillan, B. Narasimhan, D. S. Sakaguchi, A. D. Sharma, S. Zbarska, H. E. Gendelman, *Nanomed. Nanotechnol. Biol. Med.* **2015**, *11*, 715.
[12] M. E. Marti, A. D. Sharma, D. S. Sakaguchi, S. K. Mallapragada, in *Nanomaterials in Tissue Engineering*, (Eds: A. K. Gaharwar, S. Sant, M. J. Hancock and S. S. Hacking), Woodhead Publishing **2013**, p. 275.
[13] E. J. Sandquist, M. Uz, A. D. Sharma, B. B. Patel, S. K. Mallapragada, D. S. Sakaguchi, in *Neural Engineering: From Advanced Biomaterials to 3D Fabrication Techniques* (Eds: L. G. Zhang, D. L. Kaplan), Springer International Publishing, Cham, Switzerland **2016**, p. 25.
[14] G. M. Whitesides, *Nature* **2006**, *442*, 368.
[15] S.-Y. Teh, R. Lin, L.-H. Hung, A. P. Lee, *Lab Chip* **2008**, *8*, 198.
[16] F. Sharifi, B. B. Patel, A. K. Dzuilko, R. Montazami, D. S. Sakaguchi, N. Hashemi, *Biomacromolecules* **2016**, *17*, 3287.
[17] F. Sharifi, A. C. Sooriyarachchi, H. Altural, R. Montazami, M. N. Rylander, N. Hashemi, *ACS Biomater. Sci. Eng.* **2016**, *2*, 1411.
[18] F. Sharifi, S. Ghobadian, F. R. Cavalcanti, N. Hashemi, *Renewable Sustainable Energy Rev.* **2015**, *52*, 1453.
[19] P. J. Goodrich, F. Sharifi, N. Hashemi, *RSC Adv.* **2015**, *5*, 71203.
[20] N. Hashemi, J. M. Lackore, F. Sharifi, P. J. Goodrich, M. L. Winchell, N. Hashemi, *Technology* **2016**, *04*, 98.
[21] M. A. Daniele, D. A. Boyd, A. A. Adams, F. S. Ligler, *Adv. Healthcare Mater.* **2015**, *4*, 11.
[22] Y. Jun, E. Kang, S. Chae, S.-H. Lee, *Lab Chip* **2014**, *14*, 2145.
[23] F. Sharifi, D. Kurteshi, N. Hashemi, *J. Mech. Behav. Biomed. Mater.* **2016**, *61*, 530.
[24] F. Sharifi, Z. Bai, R. Montazami, N. Hashemi, *RSC Adv.* **2016**, *6*, 55343.
[25] H. Hähl, J. N. Vargas, A. Griffo, P. Laaksonen, G. Szilvay, M. Lienemann, K. Jacobs, R. Seemann, J.-B. Fleury, *Adv. Mater.* **2017**, *29*, 1602888.
[26] R. Zilionis, J. Nainys, A. Veres, V. Savova, D. Zemmour, A. M. Klein, L. Mazutis, *Nat. Protoc.* **2017**, *12*, 44.
[27] H. J. Sung, C. Meredith, C. Johnson, Z. S. Galis, *Biomaterials* **2004**, *25*, 5735.
[28] S. Temple, *Nature* **2001**, *414*, 112.
[29] F. H. Gage, *Science* **2000**, *287*, 1433.
[30] J. Zhang, X. Lu, G. Feng, Z. Gu, Y. Sun, G. Bao, G. Xu, Y. Lu, J. Chen, L. Xu, X. Feng, Z. Cui, *Cell Tissue Res.* **2016**, *366*, 129.
[31] X. Feng, X. Lu, D. Huang, J. Xing, G. Feng, G. Jin, X. Yi, L. Li, Y. Lu, D. Nie, X. Chen, L. Zhang, Z. Gu, X. Zhang, *Cell. Mol. Neurobiol.* **2014**, *34*, 859.

[32] G. T. Christopherson, H. Song, H. Q. Mao, *Biomaterials* **2009**, *30*, 556.
[33] J. B. Recknor, D. S. Sakaguchi, S. K. Mallapragada, *Biomaterials* **2006**, *27*, 4098.
[34] A. D. Sharma, S. Zbarska, E. M. Petersen, M. E. Marti, S. K. Mallapragada, D. S. Sakaguchi, *J. Biosci. Bioeng.* **2016**, *121*, 325.
[35] M. Uz, M. Buyukoz, A. D. Sharma, D. S. Sakaguchi, S. A. Altinkaya, S. K. Mallapragada, *Acta biomaterialia* **2017**, *53*, 293.
[36] S. E. Szczesny, T. P. Driscoll, H.-Y. Tseng, P.-C. Liu, S.-J. Heo, R. L. Mauck, P.-H. G. Chao, *ACS Biomater. Sci. Eng.* **2017**, *3*, 2869.
[37] Y. Liu, X. Zhang, Y. Xia, H. Yang, *Adv. Mater.* **2010**, *22*, 2454.
[38] T. Lin, H. Wang, X. Wang, *Adv. Mater.* **2005**, *17*, 2699.
[39] H. Song, C. F. Stevens, F. H. Gage, *Nature* **2002**, *417*, 39.
[40] V. Mahairaki, S. H. Lim, G. T. Christopherson, L. Xu, I. Nasonkin, C. Yu, H. Q. Mao, V. E. Koliatsos, *Tissue Eng., Part A* **2011**, *17*, 855.
[41] F. H. Gage, P. W. Coates, T. D. Palmer, H. G. Kuhn, L. J. Fisher, J. O. Suhonen, D. A. Peterson, S. T. Suhr, J. Ray, *Proc. Natl. Acad. Sci.* USA **1995**, *92*, 11879.
[42] J. Ray, D. A. Peterson, M. Schinstine, F. H. Gage, *Proc. Natl. Acad. Sci.* USA **1993**, *90*, 3602.
[43] H. J. Song, C. F. Stevens, F. H. Gage, *Nat. Neurosci.* **2002**, *5*, 438.
[44] J. C. Conover, R. Q. Notti, *Cell Tissue Res.* **2008**, *331*, 211.
[45] A. E. Wurmser, T. D. Palmer, F. H. Gage, *Science* **2004**, *304*, 1253.
[46] F. M. Watt, B. L. Hogan, *Science* **2000**, *287*, 1427.
[47] J. Oh, J. B. Recknor, J. C. Recknor, S. K. Mallapragada, D. S. Sakaguchi, *J. Biomed. Mater. Res., Part A* **2009**, *91A*, 575.
[48] S. H. Lim, X. Y. Liu, H. Song, K. J. Yarema, H. Q. Mao, *Biomaterials* **2010**, *31*, 9031.
[49] J. Yao, C. W. Ko, P. Y. Baranov, C. V. Regatieri, S. Redenti, B. A. Tucker, J. Mighty, S. L. Tao, M. J. Young, *Tissue Eng., Part A* **2015**, *21*, 1247.
[50] E. B. Lavik, H. Klassen, K. Warfvinge, R. Langer, M. J. Young, *Biomaterials* **2005**, *26*, 3187.
[51] K. Warfvinge, J. F. Kiilgaard, E. B. Lavik, E. Scherfig, R. Langer, H. J. Klassen, M. J. Young, *Arch. Ophthalmol.* **2005**, *123*, 1385.
[52] S. Tao, C. Young, S. Redenti, Y. Zhang, H. Klassen, T. Desai, M. J. Young, *Lab Chip* **2007**, *7*, 695.
[53] M. Pekny, M. Pekna, *Physiol. Rev.* **2014**, *94*, 1077.
[54] U.-K. Hanisch, H. Kettenmann, *Nat. Neurosci.* **2007**, *10*, 1387.
[55] E. Avila-Muñoz, C. Arias, *Ageing Res. Rev.* **2014**, *18*, 29.
[56] A. J. Engler, S. Sen, H. L. Sweeney, D. E. Discher, *Cell* **2006**, *126*, 677.
[57] C. M. Lo, H. B. Wang, M. Dembo, Y. L. Wang, *Biophys. J.* **2000**, *79*, 144.